Journal of Alloys and Compounds 890 (2021) 161889

Contents lists available at ScienceDirect

Journal of Alloys and Compounds

journal homepage: www.elsevier.com/locate/jalcom

Sol-gel assisted molten-salt synthesis of novel single phase $Y_{3-2x}Ca_{2x}Ta_xAl_{5-x}O_{12}$:1%Eu garnet structure phosphors

Monika Skruodiene[a,*], Ruta Juodvalkyte[b], Greta Inkrataite[b], Andrius Pakalniskis[b], Rimantas Ramanauskas[c], Anatolijs Sarakovskis[a], Ramunas Skaudzius[b]

[a] Institute of Solid State Physics, University of Latvia, 8 Kengaraga str., LV-1063 Riga, Latvia
[b] Institute of Chemistry, Faculty of Chemistry and Geosciences, Vilnius University, Naugarduko 24, LT-03225 Vilnius, Lithuania
[c] State Research Institute Center for Physical Sciences and Technology, Sauletekio av. 3, LT-10257 Vilnius, Lithuania

ARTICLE INFO

Article history:
Received 27 May 2021
Received in revised form 3 September 2021
Accepted 4 September 2021
Available online 10 September 2021

Keywords:
YAG
Ca^{2+} and Ta^{5+} doped yttrium aluminum garnet
luminescence
Co-doping
charge compensation

ABSTRACT

Strong absorption and emission are the key the features of any phosphor. The results obtained during this study demonstrate the difficulty of the incorporation of tantalum ions into the garnet structure and reveal that only the combination of Sol-Gel synthesis method together with Molten-Salt technique enable to obtain a single-phase cubic garnet structure. Note that, the Sol-Gel synthesis assisted by further processing by Molten-Salt technique can be a potentially new way of material preparation reported in literature. This work also proves that this combination of synthesis methods is much more capable of incorporating ions with large ionic radii into the garnet structure as compared to traditional Sol-Gel method. Moreover, samples synthesized using this new technique exhibit 30% higher emission intensities as compared to the ones prepared by the original Sol-Gel method, while also reducing the needed sintering temperature by 200 °C. To the best of our knowledge, the modification of yttrium aluminum garnet ($Y_3Al_5O_{12}$, YAG) by co-doping it with Ca^{2+} and Ta^{5+} ions by Sol-Gel assisted Molten-Salt route has been investigated for the first time.

1. Introduction

The growing need for light emitting diodes (LEDs) and lasers by the human society demands safe, environmentally friendly synthesis techniques for fabrication of low-cost novel materials with better and improved properties. One of the most suitable ways to solve the need for this demand is to improve the already existing compounds by modifying their chemical composition and, in such a way, tuning their already excellent properties such as quantum yield, emission color, thermal and radiation stability needed for practical applications [1–4].

Bulk yttrium aluminum garnet ($Y_3Al_5O_{12}$, YAG) doped with trivalent rare-earth ions shows optical, thermal, and physical properties comparable to its single-crystal rods, and is currently used in a wide variety of applications. Doped YAG ceramics are easier to fashion into shapes ideal for newly designed laser devices, and it is also less expensive to fabricate in large quantities. From the spectroscopic point of view, ceramics can substitute single-crystals in lasers while retaining their capabilities. The increased compositional versatility of ceramics as well as possible applications and relatively lower price of production, enables the tailoring of luminescence properties for improved laser materials. However, optical properties are strongly dependent on the synthesis procedure, crystal structure, defects, *etc.* As such, this topic still requires further in depth research [5–8].

Many different synthesis methods of synthetic garnets are described in literature, but wet-chemical processing, *e.g.*, sol-gel synthesis, is one of the leading ways. Compared to the other methods, such as solid-state, sol-gel method has significant advantages including low-cost, easy fabrication, more homogenous distribution of doped ions and lower synthesis temperatures. Nevertheless, as technology advances, there is a need for even more stable and versatile materials. Recently, molten-salt synthesis attracted more attention due to the ability to achieve phase formation at much lower temperature. A significant advantage of this method is the simplicity of the technique, which does not require a substantial investment inexpensive equipment. However, as the precursor for such reactions the mixture of powders is regularly used. To the best of our knowledge, there is no reported cases in literature that these two methods were combined [9,10].

* Corresponding author.
E-mail addresses: monika.skruodiene@cfi.lu.lv (M. Skruodiene), anatolijs.sarakovskis@cfi.lu.lv (A. Sarakovskis).

https://doi.org/10.1016/j.jallcom.2021.161889
0925-8388/

Rare-earth ions have received a lot of attention due to their intraconfigurational $4f^n$ electron transitions, as well as unique and fascinating optical properties arising from them. Rare-earth ion spectroscopy has become a trigger for new, now widely used, application areas, such as optical displays, solid-state lighting, optical temperature sensors, biomarkers, optical heaters *etc.* Phosphors doped with rare-earth ions that show specific spectral properties required for different applications are often referred to as the next generation illumination sources [11–14].

One of the most widely used activators for the emission of red light is the europium ion (Eu^{3+}). Luminescence properties of europium, similarly to other emitting ions, are strongly dependent on its concentration in the matrix and are widely studied because of their intense orange-red emission at around 590–720 nm arising from the $^5D_0 \rightarrow {}^7F_2$ to the $^5D_0 \rightarrow {}^7F_4$ transitions. Eu^{3+} ions can be easily introduced into a wide variety of different host materials making it an indispensable dopant in many efficient red phosphors. So far, it can be found in many different compound groups such as oxides, vanadates, phosphates, borates, tungstates, molybdates just to name a few [15–23].

Nowadays, research of novel garnet ceramics is focused on improvement of optical properties, such as emission intensity, quantum efficiency, decay kinetics and on their application in different areas. The aforementioned optical properties could be enhanced by suppressing charge recombination during the electron transfer processes, *via* crystal field modulation, energy transfer or charge compensation. Charge compensation is the most commonly used method because it can be easily realized. The alkali metal ions, with low oxidation states and different ionic radius, can enhance optical properties of rare-earth ion activated phosphors by co-doping method [24–29].

Doped YAG could be a perfect lasing medium due to the properties mentioned. A lot of scientific papers have been published on the wide variety of rare-earth and other trivalent ions (*e.g.*, Er^{3+}, Ho^{3+}, Tm^{3+}, Yb^{3+}, Cr^{3+}), which can be incorporated into the YAG matrix. However, one of the current challenges and a huge interest for garnet research is how to obtain a single phase YAG when it is doped with larger quantities of divalent or pentavalent ions. To the best of our knowledge, pure garnet structure of $Y_{3-2x}Ca_{2x}Ta_xAl_{5-x}O_{12}$:1%Eu, when x = 0.01–0.1 is reported here for the first time. Only the combination of Sol-Gel and Molten-Salt routes allowed for the fabrication of the single-phase products. This method was reported to synthesize graphene modified spinel structure $Li_4Ti_5O_{12}$ (for Li-ion battery anodes) composites for the first time though it was not explored for garnet structure compounds [30]. In the present work, the concentration influence of calcium(II) and tantalum(V) ions on the luminescence properties of Europium as well as the novel synthesis procedure are discussed in detail.

2. Experimental section

2.1. Synthesis procedure

The investigated phosphors were synthesized by the citric acid assisted Sol-Gel method. Yttrium nitrate ($Y(NO_3)_3{\cdot}6H_2O$, Aldrich, 99.99%), tantalum oxide (Ta_2O_5, Aldrich, 99.99%), aluminum nitrate ($Al(NO_3)_3{\cdot}9H_2O$, Roth, ≥98%), europium oxide (Eu_2O_3, Aldrich, 99.99%), were used as starting materials, potassium chloride (KCl, ACS reagent, 99.0%) was used as a flux and citric acid ($C_6H_8O_7{\cdot}H_2O$, Penta, 99.5%) as a complexing agent. Starting materials were weighed to yield compositions with formula: $Y_{3-2x}Ca_{2x}Ta_xAl_{5-x}O_{12}$, when x = 0.01–1. Nominal synthesis was performed to obtain 1 g of material.

2.2. Sol-gel route

All nitrates were dissolved in water at 70–80 °C temperature. Separately, Ta_2O_5 and Eu_2O_3 were dissolved in hot diluted nitric acid. Then nitric acid was evaporated, and distilled water was added subsequently in order to remove the excess of nitric acid. After that, the mixture of partly dissolved oxides (tantalum oxide did not fully dissolve) was poured into the initial solution of nitrates and the resulting mixture was being stirred with a magnetic stirrer for 2 h. After 2 h, the complexing agent (citric acid) at molar ratio of 1:1 was added to all metal ions. Then the formed sol was being stirred for 1 h at the same temperature, afterwards, at the room temperature for 24 h. The obtained solution was evaporated close to dryness. Finally, sol was being dried in a drying furnace at 140 °C temperature for 24 h. Porous xerogel was ground in a mortar and annealed: firstly, at 1000 °C for 2 h in air, with a 5 °C/min heating rate, in covered crucibles, secondly, the same powders were heated at 1500 °C in air for 4 h, with a 5 °C/min heating pace.

2.3. Sol-gel assisted by molten-salt route

All gels were prepared under the same conditions as it is described in Sol-Gel route section. Then the sample was calcinated at 600 °C in air for 2 h, with a 5 °C/min heating rate, in covered crucibles to remove the organic components and residual nitrates. Later it was pre-ground and mixed with flux (10:1 ratio of flux (KCl) to reagents) and sintered 1300 °C in air for 4 h, with a 5 °C/min heating rate.

2.4. Characterization

For phase identification at room temperature XRD data was collected in 15–80° 2θ range (step width of 0.01°, scan speed 10°/min, dwell time of 5.0 s) using Ni-filtered Cu Kα1 radiation on Rigaku MiniFlexII diffractometer. The measurement current and voltage were set to 15 mA and 30 kV, respectively.

Scanning electron microscopy (SEM) micrographs were taken using Hitachi SU-70 SEM. The powder was fixed on a carbon film. The proper magnification was selected, and images were recorded. The particle size measurements were done using open-source Fiji (ImageJ) software by accidently selecting random particles.

Luminescence spectra were recorded on the Edinburgh Instruments FLS980 spectrometer equipped with double excitation and emission monochromators, 450 W Xe arc lamp, a cooled (−20 °C) single-photon counting photomultiplier (Hamamatsu R928) and a lens optics for powder samples. The photoluminescence emission spectra were corrected by the correction file obtained from a tungsten incandescent lamp, certified by NPL (National Physics Laboratory, UK). The step size was 0.5 nm and the integration time was 0.2 s. Excitation wavelengths of 393.5 nm were selected, while the emission was monitored at 608.5 nm.

3. Results and discussion

X-ray diffraction (XRD) and Rietveld analysis. The synthesized samples were characterized by the XRD method in order to evaluate their phase composition and purity. The main reflexes were assigned to the garnet phase (PDF2 [00-033-0040], Entry # 96-152-9038), which means that all co-doped YAG samples possess a majority phase with cubic crystal structure, which corresponds to $Ia\bar{3}d$ (#230) space group. The diffraction patterns of samples synthesized *via* Sol-Gel route and annealed in 1500 °C are displayed in Fig. 1. For these compounds, small additional peaks were observed at around 2θ = 29°, 30.5° and 32.5° indicating the formation of an impurity

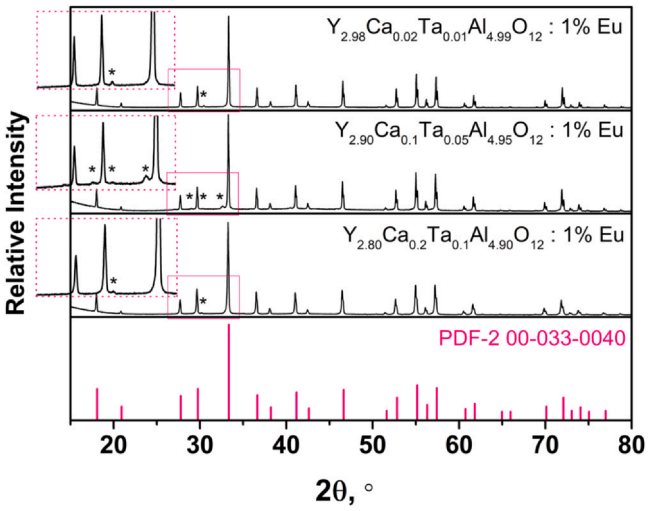

Fig. 1. XRD patterns of $Y_{3-2x}Ca_{2x}Ta_xAl_{5-x}O_{12}$:1%Eu, when x = 0.01–0.1, synthesized *via* Sol-Gel route, annealed at 1500 °C in air.

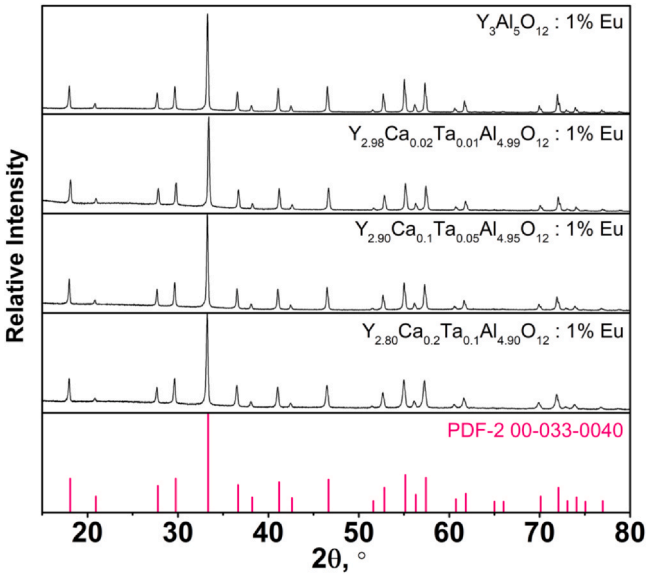

Fig. 2. XRD patterns of $Y_{3-2x}Ca_{2x}Ta_xAl_{5-x}O_{12}$: 1% Eu, when x = 0.01–0.1, synthesized *via* Sol-Gel assisted Molten-Salt route, annealed at 1300 °C in KCl, in air.

phase. Samples with x = 0.01 and x = 0.1 Ta^{5+} concentration showed peak of the secondary phase at 2θ = 30.5° and sample with x = 0.05 Ta^{5+} concentration had additional peaks at 2θ = 29°, 2θ = 30.5° and 2θ = 32.5°. These additional reflections matched well with the reference data of the monoclinic phase of Ta_2O_5 (marked "★", Entry # 96-153-9125). Fig. 2 shows diffraction patterns of samples synthesized *via* the Molten-Salt assisted Sol-Gel route and annealed at 1300 °C. Each peak present in the diffraction pattern was ascribed to the yttrium aluminum garnet phase (PDF2 [00-033-0040], Entry # 96-152-9038). No additional peaks were observed, which means, tantalum ions were successfully introduced into the garnet lattice and formation of impurity phase was avoided. Additionally, a small shift of all the peaks towards smaller 2θ values was observed. This is caused by the different ionic radii of the substituted ions and related to the variations in the unit cell parameters. Since the ionic radius of Y^{3+} and Al^{3+} are much smaller than their counterpart Ca^{2+} and Ta^{5+} [34]. From the given diffraction patterns in Fig. 1 and Fig. 2 the increase in background can be noticed. The large initial intensity of the background in the 2θ = 15° and 22° comes from the amorphous glass sample holder used during the measurements. It is also worthy to note that, if the content of tantalum exceeds x = 0.1, then the formation of different impurity phases begins. The secondary phases were identified to be the metastable orthorhombic $Ta_2O_{2.2}$ and monoclinic form of Ta_2O_5 (Appendix 1 in Supplementary material).

The more detailed structural analysis of the synthesized samples was performed using Rietveld refinement. Rietveld refinement results confirmed the formation of the secondary phase, as mentioned before, in co-doped samples, synthesized *via* Sol-Gel route. The monoclinic Ta_2O_5 phase with I121 space group in the samples when x = 0.01, 0.05, 0.1 accounts for a fraction of 3.5%, 5.6% and 2.2% of the total volume, respectively. With the increase of calcium and tantalum concentrations, the cell parameter *a* is also increasing, confirming our initial observation, even if the secondary phase starts to form (Table 1, Sol-Gel route). These results further confirm our initial assessment of Sol-Gel method being unfit for the preparation of such compounds. Meanwhile, in the case when samples were prepared by Sol-Gel assisted Molten-Salt route, Rietveld refinement analysis confirmed that there is no evidence of the secondary phase formation in the samples. With the increase of calcium and tantalum concentrations, cell parameter *a* is also gradually increasing (Table 1, Molten-Salt route), indicating that all of the added tantalum is successfully incorporated into the garnet structure, to the best of our best knowledge, for the first time. Note that, the values of the lattice parameter in the table show trends rather than absolute values. Although the lattice parameters of the compounds synthesized by Sol-Gel method are higher than those of the synthesized by Sol-Gel assisted Molten-Salt method, an error is also possible due to the impurity phase. Rietveld refined XRD patterns (observed, calculated and the difference patterns) along with the refined positional parameters were added as a supplementary file.

Table 1 represents the structural phases and unit cell parameters of synthesized samples.

Scanning electron microscopy (SEM) analysis. SEM analysis revealed the surface morphology and the particle size of the synthesized powders. All of the characterized samples possess irregular sphere-like morphology with clear boundaries between each

Table 1
Crystallographic data of synthesized samples.

Sample	Space group Garnet/Ta_2O_5	Garnet/ Ta_2O_5, %	*a*, Å (Garnet)	Vol, Å^3
Sol-Gel route	–	–	–	–
$Y_3Al_5O_{12}$:1%Eu	$Ia\bar{3}d$/-	100/-	12.005	1730
$Y_{2.98}Ca_{0.02}Ta_{0.01}Al_{4.99}O_{12}$:1%Eu	$Ia\bar{3}d$/I121	96.5/3.5	12.009	1732
$Y_{2.90}Ca_{0.10}Ta_{0.05}Al_{4.95}O_{12}$:1%Eu	$Ia\bar{3}d$/I121	94.4/5.6	12.016	1735
$Y_{2.80}Ca_{0.20}Ta_{0.10}Al_{4.90}O_{12}$:1%Eu	$Ia\bar{3}d$/I121	97.8/2.2	12.024	1738
Molten-Salt route	–	–	–	–
$Y_3Al_5O_{12}$:1%Eu	$Ia\bar{3}d$/-	100/-	12.005	1730
$Y_{2.98}Ca_{0.02}Ta_{0.01}Al_{4.99}O_{12}$:1%Eu	$Ia\bar{3}d$/-	100/0	12.007	1731
$Y_{2.90}Ca_{0.10}Ta_{0.05}Al_{4.95}O_{12}$:1%Eu	$Ia\bar{3}d$/-	100/0	12.008	1732
$Y_{2.80}Ca_{0.20}Ta_{0.10}Al_{4.90}O_{12}$:1%Eu	$Ia\bar{3}d$/-	100/0	12.018	1736

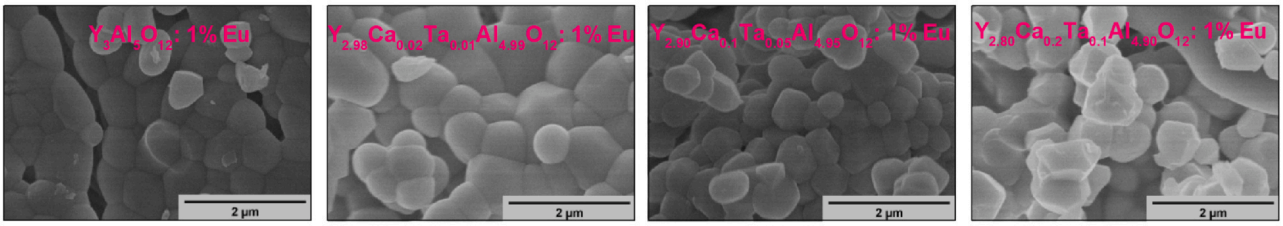

Fig. 3. SEM images of different powder the samples, synthesized *via* Sol-Gel route, annealed at 1500 °C in air.

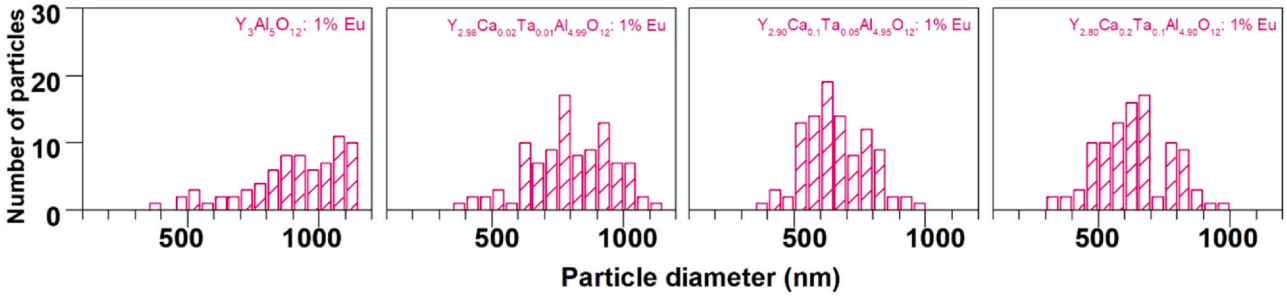

Fig. 4. Histograms of different powder the samples, annealed at 1500 °C in air.

particle especially for the samples prepared by the simple Sol-Gel method (Fig. 3.). The pores, clearly visible in Fig. 3, could have formed due to escaping gasses during decomposition of the organic components and residual nitrates (Fig. 3 and Fig. 4).

SEM micrographs of samples prepared *via* conventional Sol-Gel technique are presented in Fig. 3, while the histograms representing particle size and its distribution for these samples are given in Fig. 4. From Fig. 4 and the corresponding histograms, it is clear, that doping has no significant impact on particle size. The micro-size agglomerates maintain their clear boundaries and irregular sphere-like morphology regardless of the chemical composition. From the given histograms (Fig. 4.) it can be observed that most of the particles are in size range between 500 and 1000 nm with a broad size distribution for all the samples synthesized. A slightly different situation is observed for the particles of the samples synthesized *via* Molten-Salt route and it can be seen in Fig. 5. Although the micro-size agglomerates maintain irregular sphere-like morphology regardless of the chemical composition, the boundaries between each individual particle are harder to distinguish. From the given corresponding histograms (Fig. 6.) it can be also observed that most of the particles are in the size range between 250 and 750 nm for $Y_3Al_5O_{12}$:1%Eu and in $Y_{2.8}Ca_{0.2}Ta_{0.1}Al_{4.9}O_{12}$:1%Eu samples and 200–500 nm for $Y_{2.98}Ca_{0.02}Ta_{0.01}Al_{4.99}O_{12}$:1%Eu and $Y_{2.9}Ca_{0.1}Ta_{0.05}Al_{4.95}O_{12}$:1%Eu samples. All of the mentioned characteristics along with the broad size distribution are quite common for compounds prepared by aqueous Sol-Gel method. Note, that doped YAG samples were synthesized by different methods, and it affected a different morphology and grain size. This might cause differences in light scattering, leading to a change in the intensity of the luminescence.

Luminescence properties. The excitation spectra of $Y_{3-2x}Ca_{2x}Ta_xAl_{5-x}O_{12}$:1%Eu samples, when x = 0.01–0.1, synthesized *via* both Sol-Gel and Sol-Gel assisted Molten-Salt route, were recorded for 590 nm wavelength emission. The emission spectra of all of the samples were measured under 393.5 nm excitation wavelength light.

The excitation, emission and integrated emission spectra of the samples synthesized *via* Sol-Gel route are represented in Fig. 7. The excitation spectra contain a lot of intensive, sharp and narrow peaks associated with the *4–4f* electronic transitions of Eu^{3+} ion with a maximum being located at 394 nm ($^7F_0 \rightarrow {}^5L_6$ transition). The excitation peaks with maxima at 527 nm, 465 nm, 362 nm and 320 nm are attributed to the $^7F_0 \rightarrow {}^5D_1$, $^7F_0 \rightarrow {}^5D_2$, $^7F_0 \rightarrow {}^5D_4$ and $^7F_0 \rightarrow {}^5H_6$, transitions, respectively. A lot of low intensity peaks are observed in the range from 370 to 390 nm, which can be attributed to the $^7F_0 \rightarrow {}^5L_{6,7,8}$ and $^7F_0 \rightarrow {}^5G_{2,4,5,6}$ transitions [31]. The emission spectra (Fig. 7) show peaks at ~590 nm, ~610 nm, ~650 nm and ~710 nm, attributed to $^5D_0 \rightarrow {}^7F_1$, $^5D_0 \rightarrow {}^7F_2$, $^5D_0 \rightarrow {}^7F_3$ and $^5D_0 \rightarrow {}^7F_4$ transitions, respectively. The most intensive peak is located at ~710 nm and corresponds to $^5D_0 \rightarrow {}^7F_4$ transition. Normalized integrated emission values can be seen in Fig. 7 on the right. The integrated intensities are nearly identical, independent of the dopant concentration. It should also be noted that XRD analysis coupled with Rietveld refinement results confirmed that not all of the tantalum is introduced into the structure and the secondary phase is formed.

Fig. 8 represents luminescence spectra as well as the values of integrated emission of the samples synthesized *via* Molten-Salt route. Since the characterized samples show pure garnet structure and doping concentration of europium ions remains the same, the

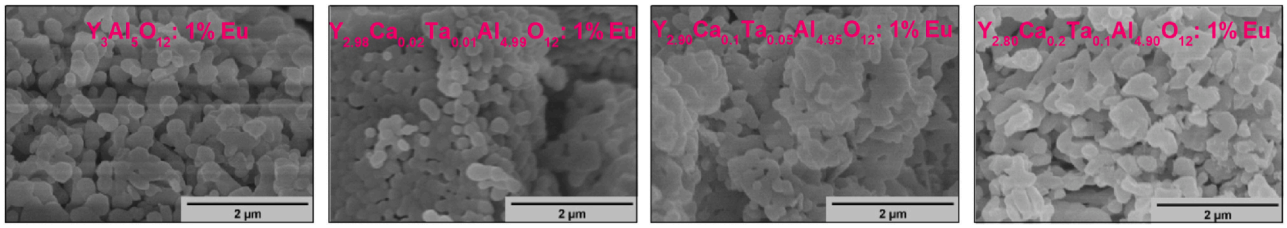

Fig. 5. SEM images of different powder the samples, synthesized *via* Molten-Salt route, annealed at 1300 °C in KCl, in air.

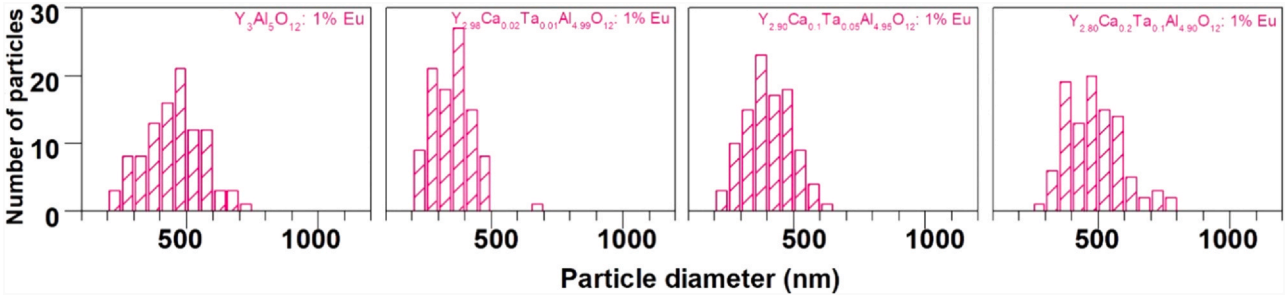

Fig. 6. Histograms of different powder the samples, synthesized *via* Molten-Salt route, annealed at 1300 °C in KCl, in air.

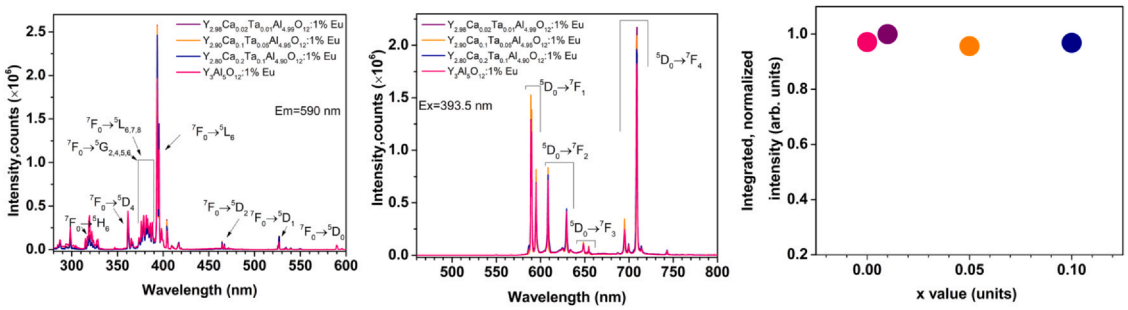

Fig. 7. Excitation (left) and emission (middle) spectra of $Y_{3-2x}Ca_{2x}Ta_xAl_{5-x}O_{12}$: 1% Eu, when x = 0.01–0.1, synthesized *via* Sol-Gel route, annealed at 1500 °C in air.

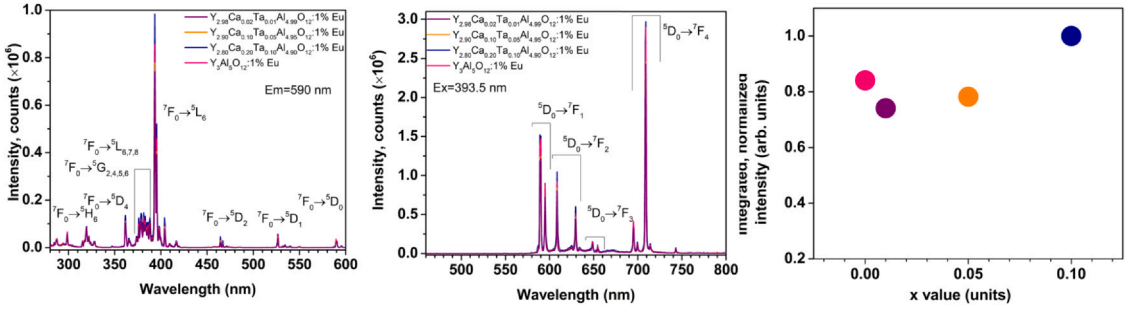

Fig. 8. Excitation (left) and emission (middle) spectra of $Y_{3-2x}Ca_{2x}Ta_xAl_{5-x}O_{12}$: 1% Eu, when x = 0.01–0.1, synthesized *via* Molten-Salt route, annealed at 1300 °C in air.

observed positions of emission and excitation peaks remain unchanged as compared to the samples prepared by Sol-Gel method [6]. By comparing emission spectra given in Figs. 7 and 8 it can be clearly seen that the samples prepared *via* Molten-Salt route show significantly more intensive luminescence (by about 30%) as compared to the samples prepared *via* conventional Sol-Gel technique. Moreover, the dopant concentration can also affect luminescence properties. $Y_{2.98}Ca_{0.02}Ta_{0.01}Al_{4.99}O_{12}$:1%Eu and $Y_{2.90}Ca_{0.10}Ta_{0.05}Al_{4.95}O_{12}$:1%Eu (Fig. 8) samples do not exhibit improved emission (integrated emission even slightly decreases), but if x = 0.1 is integrated into the structure, emission increases significantly (by 16%). To conclude, emission of europium doped garnets is affected by the insertion of tantalum and calcium, which causes the slight increase of the lattice parameter *a*. Furthermore, the changes of the local environment of luminescent dopant and difference in particle size distribution caused by doping, might be the one of the reasons for improved luminescence properties [31–33]. The CIE chromaticity is given as a supplementary material.

4. Conclusion

Based on the obtained results we can conclude that Ta and Ca co-doped YAG samples were single phase when prepared by Molten-Salt route up to x = 0.1. Further increase in dopant concentration caused formation of impurity phases. In the case of conventional Sol-gel preparation method no co-doped samples showed single phase garnet structure. Rietveld refinement data confirmed the incorporation of dopant ions into the structure as the increase in unit cell parameter *a*, since smaller ions were being replaced by larger ones. The morphology of the particles was in accordance to those typically obtained *via* Sol-Gel technique with an irregular semi-spherical shape and broad size distribution. In the case of Molten-Salt preparation, the particles showed much smaller size averaging around 400 nm with boundaries between individual particles disappearing. While the compounds prepared by the Sol-Gel technique contain a noticeable fraction of the particle with the size much larger than 750 nm and individual particles being clearly distinguished. Luminescence measurements of the obtained compounds revealed typical emission and excitation spectra for Eu^{3+}, showing presence of narrow bands arising from forbidden *4–4f* electron transitions. Sample co-doped with 0.4 of calcium and 0.2 of tantalum and prepared by Molten-Salt method showed the highest emission intensity out of all the samples by about one third. To conclude, the obtained results testify that the Sol-Gel assisted Molten-Sol method, described in this work, is a new and effective route for sample preparation. This is especially important, since aliovalent doping with large ions was achieved in no small concentrations while the optical

properties were improved. This shows that method described in this report could also be potentially applied in synthesis of many new compounds with improved properties.

CRediT authorship contribution statement

Anatolijs Sarakovskis: Conceptualization, Software, Validation, Resources, Writing – review & editing, Supervision, Funding acquisition. **Ramunas Skaudzius:** Conceptualization, Methodology, Validation, Resources, Writing – review & editing, Supervision. **Monika Skruodiene:** Formal analysis, Investigation, Data curation, Writing – original draft, Visualization, Project administration, Funding acquisition. **Ruta Juodvalkyte:** Investigation, Data curation. **Rimantas Ramanauskas:** Resources, Writing – review & editing, Supervision. **Andrius Pakalniskis:** Writing – original draft. **Greta Inkrataite:** Writing – original draft.

Declaration of Competing Interest

The authors declare that they have no known competing financial interests or personal relationships that could have appeared to influence the work reported in this paper.

Acknowledgements

The work of Monika Skruodiene is supported by ERDF PostDoc project No. 1.1.1.2/VIAA/3/19/480. Institute of Solid State Physics, University of Latvia has received funding from the European Union's Horizon 2020 Framework Programme H2020-WIDESPREAD-01-2016-2017-TeamingPhase2 under grant agreement No. 739508, project CAMART^2.

Appendix A. Supporting information

Supplementary data associated with this article can be found in the online version at doi:10.1016/j.jallcom.2021.161889.

References

[1] V. Ţucureanu, D. Munteanu, Enhanced optical properties of YAG:Ce yellow phosphor by modification with gold nanoparticles, Ceram. Int. 45 (2019) 7641–7648, https://doi.org/10.1016/j.ceramint.2019.01.061
[2] A. Boukerika, L. Guerbous, H. Chelef, L. Benharrat, Preparation and characterization of bright high quality YAG: Eu3+ thin films grown by sol–gel dip-coating technique, Thin Solid Films 683 (2019) 74–81, https://doi.org/10.1016/j.tsf.2019.05.017
[3] Y. Pan, M. Wu, Q. Su, Tailored photoluminescence of YAG:Ce phosphor through various methods, J. Phys. Chem. Solids 65 (2004) 845–850, https://doi.org/10.1016/j.jpcs.2003.08.018
[4] M.A. Almessiere, N.M. Ahmed, I. Massoudi, A.L. Al-Otaibi, A.A. Al-shehri, M. Al Shafouri, Study of the structural and luminescent properties of Ce3+ and Eu3+ co-doped YAG synthesized by solid state reaction, Optik 158 (2018) 152–163, https://doi.org/10.1016/j.ijleo.2017.12.031
[5] L.M. Calado, M.G. Taryba, M.J. Carmezim, M.F. Montemor, Self-healing ceria-modified coating for corrosion protection of AZ31 magnesium alloy, Corros. Sci. 142 (2018) 12–21, https://doi.org/10.1016/j.corsci.2018.06.013
[6] M. Elisa, B.A. Sava, I.C. Vasiliu, R.C.C. Monteiro, J.P. Veiga, L. Ghervase, I. Feraru, R. Iordanescu, Optical and structural characterization of samarium and europium-doped phosphate glasses, J. Non-Cryst. Solids 369 (2013) 55–60, https://doi.org/10.1016/j.jnoncrysol.2013.03.024
[7] A. Herrmann, S. Fibikar, D. Ehrt, Time-resolved fluorescence measurements on Eu3+- and Eu2+-doped glasses, J. Non-Cryst. Solids 355 (2009) 2093–2101, https://doi.org/10.1016/j.jnoncrysol.2009.06.033
[8] J. Hostaša, V. Nečina, T. Uhlířová, V. Biasini, Effect of rare earth ions doping on the thermal properties of YAG transparent ceramics, J. Eur. Ceram. Soc. 39 (2019) 53–58, https://doi.org/10.1016/j.jeurceramsoc.2018.04.018
[9] Q. Guo, M. Li, D. Gu, Y. Yan, K. Yue, F. Xie, C. Zhang, C. Mou, G. Peng, T. Wang, Luminescence characterizations of YAG:Ce crystal via sol-gel method for radiotherapy, Opt. Mater. 109 (2020) 110297, https://doi.org/10.1016/j.optmat.2020.110297
[10] D.E. Bugaris, H.-C. zur Loye, Materials Discovery by Flux Crystal Growth: Quaternary and Higher Order Oxides, Angewandte Chemie International Edition, 2012, https://doi.org/10.1002/anie.201102676
[11] S. Feng, H. Qin, G. Wu, H. Jiang, J. Zhao, Y. Liu, Z. Luo, J. Qiao, J. Jiang, Spectrum regulation of YAG:Ce transparent ceramics with Pr, Cr doping for white light emitting diodes application, J. Eur. Ceram. Soc. 37 (2017) 3403–3409, https://doi.org/10.1016/j.jeurceramsoc.2017.03.061
[12] F. Chi, X. Wei, S. Zhou, Y. Chen, C. Duan, M. Yin, A simple and effective method for flow cytometric study of lymphoid malignancies using needle core biopsy specimens, Cytom. Part B Clin. Cytom. 94 (2018) 637–643, https://doi.org/10.1039/c8qi00199e
[13] Z. Dai, V. Boiko, K. Grzeszkiewicz, M. Markowska, F. Ursi, J. Hölsä, M.L. Saladino, D. Hreniak, Effect of annealing temperature on persistent luminescence of Y3Al2Ga3O12:Cr3+ co-doped with Ce3+ and Pr3+, Opt. Mater. 111 (2021) 110522, https://doi.org/10.1016/j.optmat.2020.110522
[14] L. Peng, Q. Meng, W. Sun, [Effect of fcl gene for butenyl-spinosyn biosynthesis and growth of Saccharopolyspora pogona], Sheng wu Gong. cheng xue bao = Chin. J. Biotechnol. 35 (2019) 1662–1675, https://doi.org/10.1016/j.ceramint.2019.07.048
[15] M. Laguna, N.O. Nuñez, A.I. Becerro, G. Lozano, M. Moros, J.M. de la Fuente, A. Corral, M. Balcerzyk, M. Ocaña, Synthesis, functionalization and properties of uniform europium-doped sodium lanthanum tungstate and molybdate (NaLa(XO4)2, X = Mo,W) probes for luminescent and X-ray computed tomography bioimaging, J. Colloid Interface Sci. 554 (2019) 520–530, https://doi.org/10.1016/j.jcis.2019.07.031
[16] W.L. Feng, X. Qin, P. Su, Synthesis, photoluminescence and theoretical explanations of trivalent europium-doped dipotassium tungstate phosphors, Optik 131 (2017) 1007–1015, https://doi.org/10.1016/j.ijleo.2016.12.017
[17] H. Zhou, N. Guo, Q. Liang, Y. Ding, Y. Pan, Y. Song, R. Ouyang, Y. Miao, B. Shao, Novel ratiometric optical thermometry based on dual luminescent centers from europium doped LiCa3MgV3O12 phosphor, Ceram. Int. 45 (2019) 16651–16657, https://doi.org/10.1016/j.ceramint.2019.05.207
[18] D.E. Wagner, K.M. Eisenmann, A.L. Nestor-Kalinoski, S.B. Bhaduri, A microwave-assisted solution combustion synthesis to produce europium-doped calcium phosphate nanowhiskers for bioimaging applications, Acta Biomater. 9 (2013) 8422–8432, https://doi.org/10.1016/j.actbio.2013.05.033
[19] M. Sołtys, J. Janek, L. Zur, J. Pisarska, W.A. Pisarski, Compositional-dependent europium-doped lead phosphate glasses and their spectroscopic properties, Opt. Mater. 40 (2015) 91–96, https://doi.org/10.1016/j.optmat.2014.11.052
[20] V. Hegde, A. Wagh, H. Hegde, C.S.D. Vishwanath, S.D. Kamath, Spectroscopic investigation on europium doped heavy metal borate glasses for red luminescent application, Appl. Phys. A 123 (2017) 302, https://doi.org/10.1007/s00339-017-0914-5
[21] M. Bettinelli, A. Speghini, M. Ferrari, M. Montagna, Spectroscopic investigation of zinc borate glasses doped with trivalent europium ions, J. Non-Cryst. Solids 201 (1996) 211–221, https://doi.org/10.1016/0022-3093(96)00134-2
[22] S.Z. Shmurak, A.P. Kiselev, D.M. Kurmasheva, B.S. Red'kin, V.V. Sinitsyn, Effect of solid-phase amorphization on the spectral characteristics of europium-doped gadolinium molybdate, J. Exp. Theor. Phys. 110 (2010) 759–768, https://doi.org/10.1134/S1063776110050055
[23] V.V. Shinde, A. Tiwari, S.J. Dhoble, Synthesis of RE3+ (RE3+ = Ce3+, Dy3+, Eu3+ and Tb3+) activated Gd2SiO5 optoelectronics materials for lighting, J. Mol. Struct. 1217 (2020) 128397, https://doi.org/10.1016/j.molstruc.2020.128397
[24] V. Thangadurai, W. Weppner, Effect of sintering on the ionic conductivity of garnet-related structure Li5La3Nb2O12 and In- and K-doped Li5La3Nb2O12, J. Solid State Chem. 179 (2006) 974–984, https://doi.org/10.1016/j.jssc.2005.12.025
[25] J. Xue, Y. Guo, B.K. Moon, S.H. Park, J.H. Jeong, J.H. Kim, L. Wang, Improvement of photoluminescence properties of Eu3+ doped SrNb2O6 phosphor by charge compensation, Opt. Mater. 66 (2017) 220–229, https://doi.org/10.1016/j.optmat.2017.02.002
[26] J. Huang, J. Xu, H. Luo, X. Yu, Y. Li, Effect of alkali-metal ions on the local structure and luminescence for double tungstate compounds AEu(WO4)2 (A = Li, Na, K), Inorg. Chem. 50 (2011) 11487–11492, https://doi.org/10.1021/ic2013528
[27] X. Wang, Z. Zhao, Q. Wu, Y. Li, Y. Wang, Synthesis, structure and photoluminescence properties of Ca2LuHf2(AlO4)3:Ce3+, a novel garnet-based cyan light-emitting phosphor, J. Mater. Chem. C. 4 (2016) 11396–11403, https://doi.org/10.1039/c6tc03933b
[28] S.P. Kammampata, R.H. Basappa, T. Ito, H. Yamada, V. Thangadurai, Microstructural and electrochemical properties of alkaline earth metal-doped Li garnet-type solid electrolytes prepared by solid-state sintering and spark plasma sintering methods, ACS Appl. Energy Mater. 2 (2019) 1765–1773, https://doi.org/10.1021/acsaem.8b01899
[29] V. Thangadurai, W. Weppner, Li6ALa2Nb2O12 (A=Ca, Sr, Ba): a new class of fast lithium ion conductors with garnet-like structure, J. Am. Ceram. Soc. 88 (2005) 411–418, https://doi.org/10.1111/j.1551-2916.2005.00060.x
[30] Q. Guo, Q. Wang, G. Chen, Q. Shen, B. Li, Enhancing the electrochemistry performance of Li4Ti5O12for Li-ion battery anodes by a sol–gel assisted molten salt method and graphene modification, RSC Adv. 6 (2016) 110032–110039, https://doi.org/10.1039/C6RA19938K
[31] R. Skaudžius, D. Enseling, M. Skapas, A. Selskis, E. Pomjakushina, T. Jüstel, A. Kareiva, C. Rüegg, Europium–enabled luminescent single crystal and bulk YAG and YGG for optical imaging, Opt. Mater. 60 (2016) 467–473, https://doi.org/10.1016/j.optmat.2016.08.032
[32] T. Gavrilović, J. Periša, J. Papan, K. Vuković, K. Smits, D.J. Jovanović, M.D. Dramićanin, Particle size effects on the structure and emission of Eu3+:LaPO4 and EuPO4 phosphors, J. Lumin. 195 (2018) 420–429, https://doi.org/10.1016/j.jlumin.2017.12.002
[33] S. Fu, J. Tan, X. Bai, S. Yang, L. You, Z. Du, Hybrid assembly toward enhanced thermal stability of virus-like particles and antibacterial activity of polyoxometalates, ACS Appl. Mater. Interfaces 10 (2018) 6137–6145, https://doi.org/10.1016/j.optmat.2017.11.021
[34] R.D. Shannon, Revised effective ionic radii and systematic studies of interatomic distances in halides and chalcogenides, Acta Crystallogr. Sect. A 32 (1976) 751–767, https://doi.org/10.1107/S0567739476001551